

**Orientational pinning of the vortex lattice to the crystalline lattice in a weakly pinned
Co_{0.0075}NbSe₂ single crystal**

Somesh Chandra Ganguli, Harkirat Singh, Rini Ganguly, Vivas Bagwe, Arumugam Thamizhavel
and Pratap Raychaudhuri^a

*Department of Condensed Matter Physics and Materials Science, Tata Institute of Fundamental
Research, Homi Bhabha Road, Colaba, Mumbai 400005, India.*

We report experimental evidence of strong orientational coupling between the crystal lattice and the vortex lattice in a weakly pinned Co-doped NbSe₂ single crystal through direct imaging using low temperature scanning tunneling microscopy/spectroscopy. At low fields, when the magnetic field is applied along the six-fold symmetric *c*-axis of the NbSe₂ crystal, the equilibrium configuration of the vortex lattice is preferentially aligned along the basis vectors of the crystal lattice. The orientational coupling between the vortex lattice and crystal lattice becomes more pronounced as the magnetic field is increased. We show that this coupling enhances the stability of the orientational order of the vortex lattice, which persists even in the disordered state at high fields where dislocations and disclinations have destroyed the topological order.

^a pratap@tifr.res.in

The vortex lattice (VL) in a type II superconductor provides a versatile model system to study the interplay of interaction and pinning^{1,2,3}. So far, most description of the vortex state in homogeneous 3 dimensional (3D) superconductors involves the vortex-vortex interaction, which stabilize a hexagonal Abrikosov vortex lattice, and random pinning of vortices by crystalline defects, which tend to destroy this order by pinning the vortices at random positions^{4,5,6,7}. For weakly pinned Type II superconductors, these theories predict that the topological defect free VL undergoes an order to disorder transition (ODT) through proliferation of topological defects⁸ (TD) as one approaches the superconductor-normal metal phase boundary. These TD relax the hexagonal order which makes it easier for vortices to accommodate the random pinning potential thereby enhancing the effective pinning. Thus the ODT manifests as a sharp increase in the critical current or a decrease in the real part of ac susceptibility (χ'), the so called “peak effect”⁹, which has been widely studied in weakly pinned superconducting crystals^{1,10}.

In principle, the VL can also couple with the symmetry of an underlying substrate. In superconductors with artificially engineered periodic pinning, this coupling has been shown to give rise to interesting matching effects, where the VL gets oriented in specific orientations with respect to the pinning potential when the lattice constant is commensurate with the pinning potential¹¹. However, in single crystals, the underlying symmetry of the crystal lattice (CL) is not believed to significantly influence the VL since interatomic spacing is much smaller than the size of the vortex core. Thus barring one exception,¹² most theories consider the VL to be decoupled from the CL except for the random pinning potential created by defects which hinders the relative motion between two. However, recent neutron diffraction experiments¹³ on Nb single crystal show that the structure of the VL varies depending on the symmetry of the axis along which the magnetic field is applied. Therefore the influence of the symmetry of the CL on the VL and consequently its effect on the ODT needs to be explored further.

To address this issue we performed experiments in a weakly pinned $\text{Co}_{0.0075}\text{NbSe}_2$ single crystal¹⁴ ($T_c \approx 5.9\text{K}$) by simultaneously imaging the VL and CL using a home-built low temperature scanning tunneling microscope (STM)¹⁵ operating down to 350 mK. It has been shown that small amount of Co doping in NbSe_2 decreases the anisotropy of the upper critical field, thereby effectively making the pinning weaker than its undoped counterpart¹⁶. The central result of this paper is that when the magnetic field is applied along the six-fold symmetric c -axis

of the crystal, the VL is always preferentially oriented along the unit cell vector in the layer. This orientational pinning of the VL with the crystal lattice provides a backbone for the robust orientational order of the VL across the ODT.

Prior to STM measurements the crystal is cleaved *in-situ*, resulting in atomically smooth facets several microns across. NbSe₂ has a layered hexagonal crystal structure with each unit cell consisting of two sandwiches of hexagonal Se-Nb-Se layers. Thus the crystal cleaves between the weakly coupled neighboring Se layer exposing the hexagonal Se terminated surface. Fig. 1(a) shows a high resolution topographic image (along with its Fourier transform (FT)) of the surface showing the individual selenium atoms. The 3×3 charge density wave (CDW) modulation is also visible though it is blurred due to the presence Co dopant atoms. The FT shows 6 symmetric sharp Bragg peaks corresponding to the Se lattice and 6 diffuse spots corresponding to the CDW. All VL images are acquired on the same cleaved facet.

We first focus on the VL created at a relatively low field of 2.5 kOe in the zero field cooled state (ZFC) where the magnetic field is applied after cooling the sample to the lowest temperature. The VL is imaged by measuring the tunneling conductance ($G(V) = dI/dV$) over the surface at a fixed bias voltage ($V \sim 1.2$ mV) close to the superconducting energy gap, such that each vortex core manifests as a local minimum in $G(V)$. Fig. 1(c)-(e) show representative images of the ZFC VL at 350 mK imaged over $1.5 \mu\text{m} \times 1.5 \mu\text{m}$ on three different areas of the surface. To identify topological defects, we Delaunay triangulate¹⁷ the VL and determine the nearest neighbor coordination for each flux lines. We observe that the VL is oriented along different directions at different locations with no apparent relation with the orientation of the crystalline lattice. In addition, in Fig. 1(e) we observe a domain boundary created by a line of dislocations (pairs of adjacent lattice points with 5-fold and 7-fold coordination), with the VL having different orientation on two sides of the boundary. These observations are consistent with earlier Bitter decoration experiments¹⁸ where large area images of the ZFC VL revealed large randomly oriented domains, albeit at much lower fields.

We now investigate whether such randomly oriented domains represent the equilibrium state of the VL. It has been shown that shaking the VL through a small magnetic perturbation, forces the system out of metastable states causing a dynamic transition to its equilibrium configuration^{19,20,21}. In our case, we did not observe any change when the ZFC VL is perturbed at

350 mK with a magnetic field pulse of 300 Oe (by ramping the field up and then down). However, when the pulse is applied after heating the sample to a temperature higher than 1.5 K the VL gets oriented along the orientation of the crystal lattice (Fig. 1(f)-(h)). For the VL in Fig. 1(e), in addition this process annihilates the domain boundary. We also observed that the orientation of the VL does not change when the crystal is heated up to 4.5 K without applying the pulse. Therefore, the domain structure in the ZFC VL corresponds to a metastable state, where different parts of the VL get locked in different orientations.²² To explore if this orientational ordering leaves its signature on the bulk pinning properties of the VL we performed ac susceptibility measurements on the same crystal (Fig. 1(b)) using three protocols: In the first two protocols, the VL is prepared in the FC and ZFC state respectively (at 2.5 kOe) and the real part of susceptibility (χ') is measured while increasing the temperature; in the third protocol the vortex lattice is prepared at the lowest temperature in the ZFC state and the χ' -T is measured while a magnetic field pulse of 300 Oe is applied intervals 100 mK while warming up. As expected the disordered FC state has a stronger diamagnetic shielding response than the ZFC state representing stronger bulk pinning. For the pulsed-ZFC state, χ' -T gradually diverges from the ZFC warmed up state and shows a weaker diamagnetic shielding response and exhibits a more pronounced dip at the peak effect. Both these show that the pulsed-ZFC state is more ordered than the ZFC warmed up state, consistent with the annihilation of domain walls with magnetic field pulse.

We now investigate the orientation of a single domain as the magnetic field is increased. Fig. 2 (a)-(d) shows the VL at the same position for 4 different fields when the magnetic field is ramped up from 2.5 kOe to 15 kOe at 350 mK. We observe that the ZFC VL gradually orients towards the crystal lattice with increase in field and above 10 kOe becomes fully oriented along the crystal lattice (Fig 2(e)). At 10 kOe, images taken at various locations of the sample surface shows that this orientation is global and no domain boundaries are observed in the ZFC VL till the onset of the ODT. As the field is increased further the VL remains topologically ordered up to 24 kOe. At 26 kOe dislocations proliferate in the VL, in the form of neighboring sites with 5-fold and 7-fold coordination. At 28 kOe, we observe that the disclinations proliferate into the lattice. However, the corresponding FT show a six-fold symmetry all through the sequence of disordering of the VL. Comparing the orientation of the principal reciprocal lattice vectors with the corresponding ones of the FT of crystal lattice, we observe that the VL is always oriented along the crystal lattice direction. In contrast to our previous studies²⁰, here an isotropic amorphous

vortex glass phase is not realized even after the disclinations have proliferated in the system. This difference reflects the weaker defect pinning in the present crystal¹⁴, which enhances the effect of orientational coupling in maintaining the orientation of the VL along the crystal lattice.

The pertinent question arising from our experiments is, what is the origin of this orientational coupling? Conventional pinning cannot explain these observations, since it requires a modulation of the superconducting order parameter over a length scale of the order of the size of the vortex core, which is an order of magnitude larger than the interatomic separation and the CDW modulation in NbSe₂. One likely origin of orientational pinning is from anisotropic vortex cores whose orientation is locked along a specific direction of the crystal lattice. Since the interaction between the vortices in such a situation would be anisotropic, the interaction energy would get minimized for a specific orientation of the VL with respect to the crystal lattice. Such anisotropic vortex core can arise from several origins. In unconventional superconductors (e.g. (La,Sr)CuO₄, CeCoIn₅), the shape of the vortex core is expected to mimic the pairing symmetry of the superconducting order parameter^{23,24}. In an s-wave superconductor anisotropic vortex core could arise when the Fermi surface is anisotropic, which is believed to give rise to a square vortex core²⁵ in YNi₂B₂C and a transition from triangular to square vortex lattice with increasing magnetic field²⁶. In NbSe₂, earlier STS experiments showed that the vortex core has a hexagonal star shape structure^{27,28}, which would reinforce the hexagonal order but also preferentially orient the hexagonal VL along certain crystal lattice directions, consistent with our experiments.

In conclusion, we have used direct imaging of the crystal lattice and the VL using STM/S to show that the orientation of the VL in a conventional s-wave superconductor is strongly pinned to the crystal lattice. This orientational pinning influences both the equilibrium state at low fields and the order-disorder transition at high field. The orientational pinning could also give interesting VL states when the crystal lattice does not have hexagonal symmetry. We hope that future theories will explore the effect of this orientational pinning on the vortex phase diagram of Type II superconductors.

Acknowledgements: This work was supported by Department of Atomic Energy, Government of India.

References

-
- ¹ M. J. Higgins and S. Bhattacharya, *Physica C* **257**, 232-254 (1996).
- ² Y. Paltiel, *et al.*, *Nature* **403**, 398-401 (2000).
- ³ I. Guillamón, *et al.*, *Nat. Phys.* **10**, 851-856 (2014).
- ⁴ D. S. Fisher, M. P. A. Fisher and D. A. Huse, *Phys. Rev. B* **43**, 130-159 (1991).
- ⁵ T. Giamarchi and P. Le Doussal, *Phys. Rev. B* **52**, 1242-1270 (1995).
- ⁶ G. I. Menon, *Phys. Rev. B* **65**, 104527 (2002).
- ⁷ J. Kierfeld, and V. Vinokur, *Phys. Rev. B* **69**, 024501 (2004).
- ⁸ V. Vinokur *et al.* *Physica C* **295**, 209 (1998).
- ⁹ G. D'Anna *et al.* *Physica C* **218**, 238-244 (1993).
- ¹⁰ I. K. Dimitrov *et al.*, *Phys. Rev. Lett.* **99**, 047001 (2007); M. Hilke, S. Reid, R. Gagnon, and Z. Altounian, *Phys. Rev. Lett.* **91**, 127004 (2003); M. Pissas, S. Lee, A. Yamamoto, and S. Tajima, *Phys. Rev. Lett.* **89**, 097002 (2002); K Ghosh *et al.*, *Phys. Rev. Lett.* **76**, 4600 (1996).
- ¹¹ I. Guillamón *et al.*, *Nat. Phys.* **10**, 851-856 (2014).
- ¹² J. Toner, *Phys. Rev. Lett.* **66**, 2523 (1991); also see E. M. Chudnovsky, *Phys. Rev. Lett* **67**, 1809 (1991) and J. Toner, *Phys. Rev. Lett* **67**, 1810 (1991).
- ¹³ M. Laver *et al.*, *Phys. Rev. Lett.* **96**, 167002 (2006).
- ¹⁴ See supplementary material, Section II, for a.c. susceptibility measurements with and without magnetic field.
- ¹⁵ A. Kamlapure *et al.* *Rev. Sci. Instrum.* **84**, 123905 (2013).
- ¹⁶ M. Iavarone *et al.*, *Phys. Rev. B* **78**, 174518 (2008).
- ¹⁷ Details of processing of the VL images and Delaunay triangulation are given in ref. 20.
- ¹⁸ Y. Fasano *et al.* *Phys. Rev. B* **66**, 020512(R) (2002).
- ¹⁹ S. S. Banerjee *et al.*, *Appl. Phys. Lett.* **74**, 126-128 (1999).
- ²⁰ S. C. Ganguli, S. *et al.*, *Sci. Rep.* **5**, 10613 (2015).
- ²¹ G. Pasquini, D. Pérez Daroca, C. Chilotte, G. S. Lozano, and V. Bekeris, *Phys. Rev. Lett.* **100**, 247003 (2008).
- ²² Although a pulse of 300 Oe does not alter the ZFC state at 350 mK, the VL get aligned with the CL when cycled through a higher field. For details see supplementary material, Section II.

-
- ²³ M. P. Allan *et al.*, *Nat. Phys.* **9**, 468 (2013); B. B. Zhou *et al.*, *Nat. Phys.* **9**, 474 (2013).
- ²⁴ R. Gilardi *et al.*, *Phys. Rev. Lett.* **88**, 217003 (2002).
- ²⁵ H. Nishimori, K. Uchiyama, S. Kaneko, A. Tokura, H. Takeya, K. Hirata and N. Nishida, *J. Phys. Soc. Jpn.* **73**, 3247 (2004).
- ²⁶ D. McK. Paul *et al.*, *Phys. Rev. Lett.* **80**, 1517 (1998).
- ²⁷ H. F. Hess, R. B. Robinson, and J. V. Waszczak, *Phys. Rev. Lett.* **64**, 2711 (1990).
- ²⁸ I. Guillamon, H. Suderow, S. Vieira, P. Rodiere, *Physica C* **468**, 537 (2008).

Figure captions

Figure 1. (a) Topographic image of the $\text{Co}_{0.0075}\text{NbSe}_2$ crystal surface (left) and the corresponding Fourier transform (FT) (right); the direction of the basis vectors in the hexagonal crystal lattice plane comprising of selenium atoms are shown with green arrows. The Bragg spots corresponding to the atomic lattice and CDW in the FT and shown by arrows. We use the convention $(\text{length})^{-1}$ for the scale-bar on the FT. The image is acquired in constant current mode, with tunneling current of 150 pA and voltage bias of 10 mV. (b) Susceptibility (χ') as a function of temperature (T) measured at 2.5 kOe while warming up the sample from the lowest temperature. The three curves correspond to χ' -T measured after field cooling the sample (FC-W), after zero field cooling the sample (ZFC-W) and zero field cooling the sample and then applying a magnetic pulse of 300 Oe at temperature intervals of 0.1 K while warming up (pulsed ZFC-W). The y-axis is normalized to the FC-W χ' at 1.9 K. The measurements are done at 60 kHz using an a.c. excitation field of 10 mOe. (c)-(e) Conductance maps showing the ZFC VL images ($1.5 \mu\text{m} \times 1.5 \mu\text{m}$) recorded at 350 mK, 2.5 kOe at three different places on the crystal surface. (f)-(h) VL images at the same places as (c)-(e) respectively after heating the crystal to 1.5 K (for (f)) or 2 K ((g) and (h)) and applying a magnetic pulse of 300 Oe. Solid lines joining the vortices show the Delaunay triangulation of the VL and sites with 5-fold and 7-fold coordination are shown as red and white dots respectively. The direction of the basis vectors of the VL are shown by yellow arrows. In figure (e) a line of dislocations separate the VL into two domains with different orientations.

Figure 2. VL images at the same location on the sample surface imaged at (a) 2.5 kOe, (b) 5 kOe, (c) 7.5 kOe and (d) 15 kOe; the images are recorded while ramping up the field after cooling the sample to 350 mK in zero magnetic field. Solid lines joining the vortices show the Delaunay

triangulation of the VL. The yellow arrow shows the direction of one basis vector of the hexagonal VL. For reference, the direction of the corresponding basis vector of the crystal lattice is shown by green arrow. While all images were acquired over $1 \mu\text{m} \times 1 \mu\text{m}$, the image at 15 kOe has been zoomed to show around 600 vortices for clarity. (e) Angle between the orientation of the VL and the crystal lattice ($\Delta\theta$) as a function of magnetic field.

Figure 3. (a) FT of the crystal lattice; the directions of the principal reciprocal lattice vectors are shown with green arrow. (b)-(d) VL lattice images at 22, 26 and 28 kOe (left) along with their FT (right); Delaunay triangulation of the VL are shown as solid lines joining the vortices and sites with 5-fold and 7-fold coordination are shown as red and white dots respectively. The disclinations (unpaired 5-fold or 7-fold coordination sites) observed at 26 and 28 kOe are highlighted with green and purple circles. The directions of the principal reciprocal lattice vectors are shown with yellow arrows.

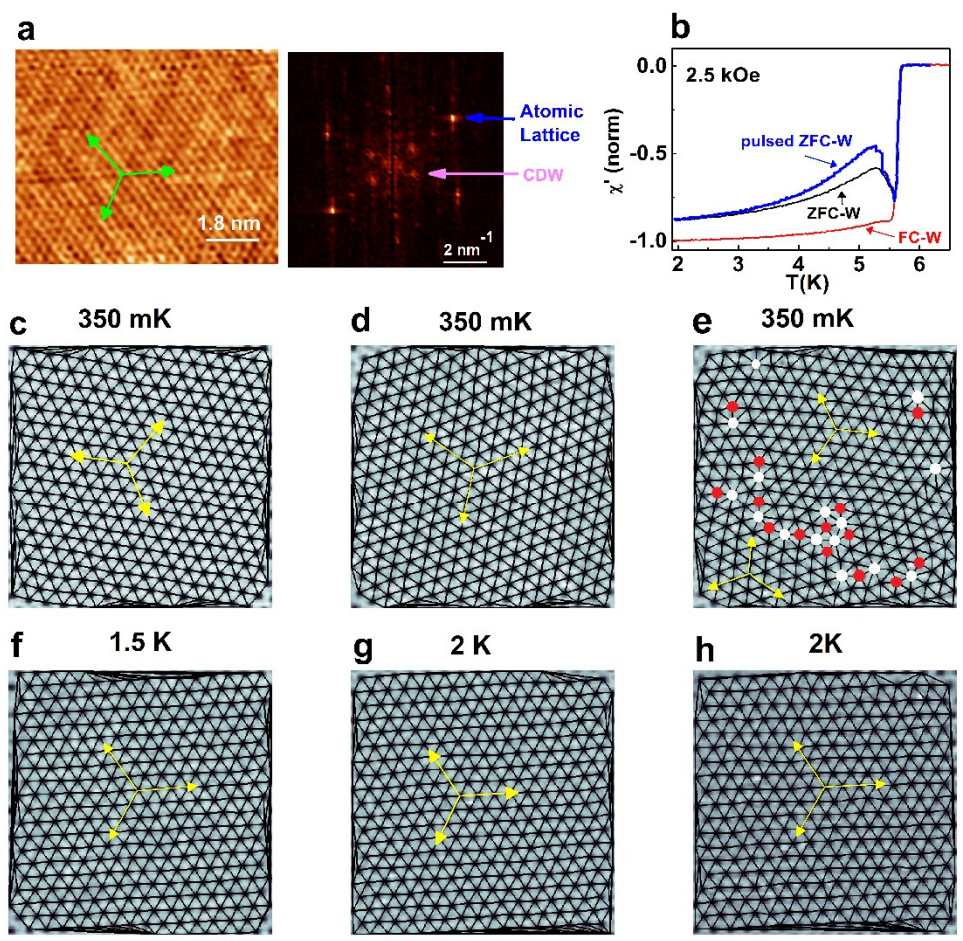


Figure 1

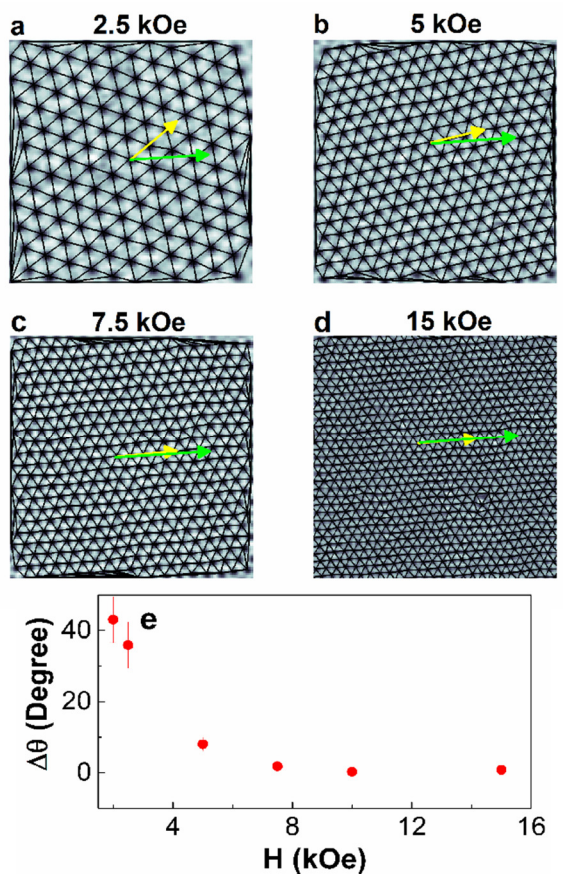


Figure 2

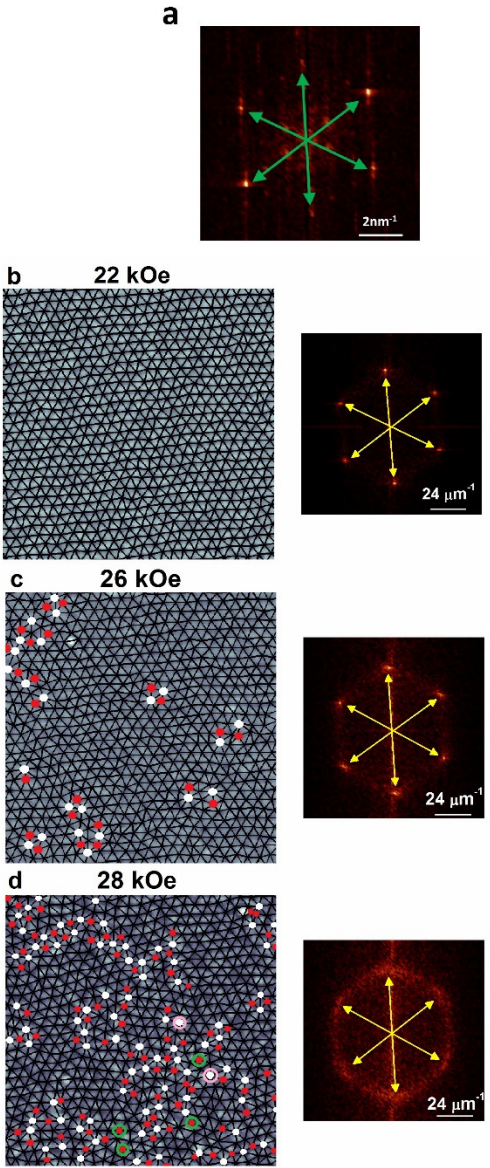


Figure 3

Supplementary Information

Orientalional pinning of the vortex lattice to the crystalline lattice in a weakly pinned $\text{Co}_{0.0075}\text{NbSe}_2$ single crystal

Somesh Chandra Ganguli, Harkirat Singh, Rini Ganguly, Vivas Bagwe, Arumugam Thamizhavel and Pratap Raychaudhuri²

Department of Condensed Matter Physics and Materials Science, Tata Institute of Fundamental Research, Homi Bhabha Road, Colaba, Mumbai 400005, India.

A. Bulk characterization of $\text{Co}_{0.0075}\text{NbSe}_2$ crystal using a.c. susceptibility

The superconducting $\text{Co}_{0.0075}\text{NbSe}_2$ crystal was characterized using a home built a.c. susceptometer operating at 60 kHz. The amplitude of the a.c. signal was fixed at 10 mOe. The linearity of the response was previously verified¹ that for this amplitude.

Fig. 1S shows the real and imaginary part (χ' and χ'') of a.c. susceptibility in zero field. The crystal shows a sharp superconducting transition with $T_c \sim 5.9$ K. The transition temperature is higher than the sample with the same nominal composition studied in ref. 20, showing that the crystal is less disordered.

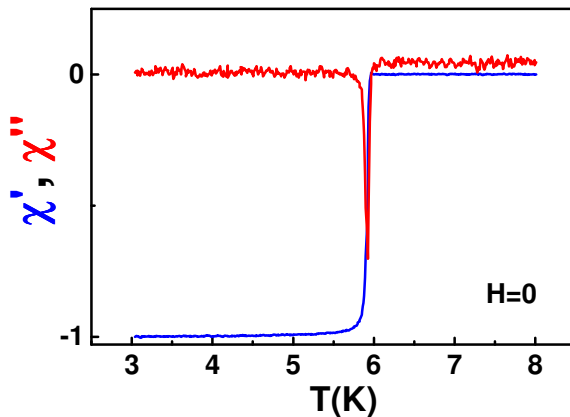


Figure 1S. Real (χ') and imaginary (χ'') part of a.c. susceptibility of the $\text{Co}_{0.0075}\text{NbSe}_2$ crystal in zero field. Both curves are normalized to the χ' value at 3 K.

To characterize the bulk VL response χ' was measured as a function of magnetic field (H) at 1.9 K after cooling the crystal in zero magnetic field. Fig. 2S shows χ' -H for increasing and decreasing field. We observe a pronounced peak effect associated with the ODT, with the χ' reaching a

² pratap@tifr.res.in

minimum at $H_p \sim 25$ kOe. The increasing and decreasing curves overlap with each other except close to the peak effect as reported previously in ref. 1. The χ' -T measured for the ZFC state prepared at 1.9 K (in a field of 5 kOe) also shows a sharp peak effect close to the superconducting transition temperature. Consistent with the higher T_c the peak effect is also sharper compared to ref. 1 showing that the crystal is cleaner and hence more weakly pinned.

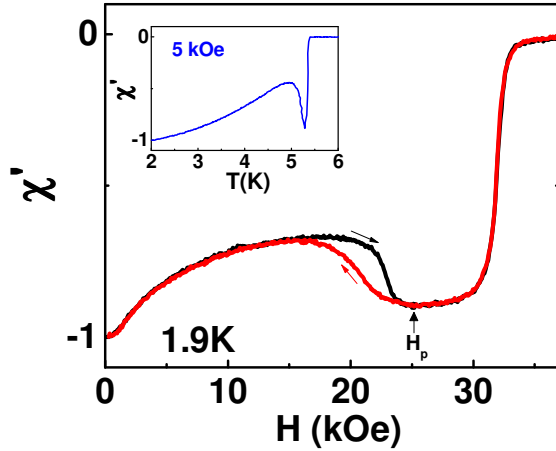


Figure 2S. Magnetic field variation of the real part of a.c. susceptibility (χ') normalized to the zero field value, at 1.9 K. The black and red curves correspond to increasing and decreasing fields respectively. (*inset*) Temperature variation of χ' at 5 kOe.

B. Reorientation of the VL at 350 mK with magnetic field cycling

The ZFC VL at 350 mK gets aligned along the CL when the crystal cycled through a high field. Fig. 3S show the evolution of the VL initially prepared in the ZFC state, as the magnetic field is increased to 7.5 kOe and then decreased back to 2.5 kOe. The VL gradually aligns along the CL as the magnetic field is increased up to 7.5 kOe. Upon decreasing the field the VL remains oriented along the CL.

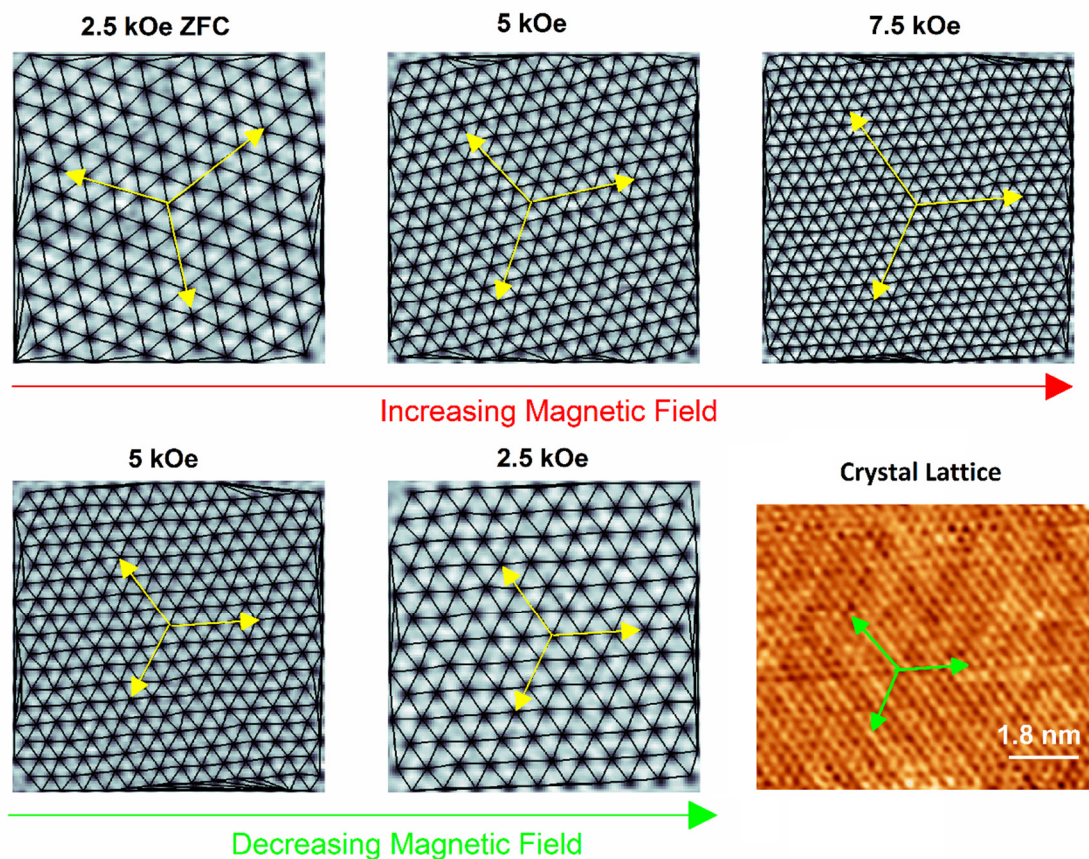


Figure 3S. The 3 upper panels show the reorientation of the VL along the CL as the magnetic field is increased from 2.5 kOe to 7.5 kOe. The 2 bottom panels starting from left show the VL as when the magnetic field is reduced. The yellow arrows show the directions of the basis vectors of the VL. For reference the crystal lattice is shown in the bottom right corner. The orientation of the basis vectors of the CL are shown by green arrows.

¹ S. C. Ganguli, S. *et al.*, *Sci. Rep.* **5**, 10613 (2015).